

Second-Order Susceptibility Terms in Orthoferrites at Room Temperature*

G. GORODETSKY AND D. TREVES

Department of Electronics, The Weizmann Institute of Science, Rehovoth, Israel

(Received 22 January 1964)

Two possible mechanisms for weak ferromagnetism, single-ion magnetocrystalline anisotropy and antisymmetric exchange, are examined on orthoferrites which contain a paramagnetic rare earth. The study was done by comparing the ferromagnetic components and the terms of the second-order susceptibility tensor that are obtained from torque measurements to the equivalent values calculated from Hamiltonians based on above mechanisms. The results show that the weak ferromagnetism is due mainly to the antisymmetric exchange mechanism.

INTRODUCTION

RARE-EARTH orthoferrites with the composition $M^{3+}Fe^{3+}O_3$, where M^{3+} stands for a rare-earth ion, exhibit weak ferromagnetism.¹⁻⁸ The orthorhombic unit cell of these compounds contains four distorted perovskite units and belongs to the space group^{9,10} D_{2h}^{16} . Both magnetic ions, Fe^{3+} , M^{3+} , lie on approximately simple cubic sublattices.^{9,10} Studies with neutron diffraction on some orthoferrites^{11,12} have shown that the crystallographic and magnetic unit cells are identical. Therefore, every unit cell contains four equivalent Fe^{3+} ions which, on the basis of experimental evidence,^{13,14} can be considered as lying in two sublattices that are approximately antiferromagnetic. A two sublattices approximation will be used from here on. In all the orthoferrites, except $SmFeO_3$, the antiferromagnetic axis is the x axis and the ferromagnetic moment is parallel to the z axis. In $SmFeO_3$ the situation is reversed.⁶

Dzyaloshinsky¹⁵ explained the appearance of the ferromagnetic components from symmetry considerations.

Moriya¹⁶ proposed two types of interaction to explain quantitatively weak ferromagnetism: (1) Single-ion magnetocrystalline anisotropy (S.I.A.); (2) Antisymmetric exchange energy (A.S.E.). In the first mechanism, from a macroscopical point of view, the

two magnetization sublattices have different easy directions. This causes a perturbation from a pure antiferromagnetic state and the appearance of weak ferromagnetism. In the second one the canting is produced by a coupling of the form, $-\mathbf{D} \cdot (\boldsymbol{\sigma}_1 \times \boldsymbol{\sigma}_2)$ which is minimum when the magnetization vectors of the two sublattices $\boldsymbol{\sigma}_1$, $\boldsymbol{\sigma}_2$ and the constant vector \mathbf{D} , are perpendicular to each other. \mathbf{D} is parallel to the y axis in all the rare-earth orthoferrites.¹⁴

The method to examine which of the models is the dominating one was developed by Treves¹⁴ and essentially the same technique is used here.

The energy E of the crystal at low static/magnetic field can in general be written as a power series:

$$E = \text{constant} + \sum_i \sigma_i(0)H_i + \frac{1}{2} \sum_{ij} x_{ij}H_iH_j + \frac{1}{6} \sum_{ijk} C_{ijk}H_iH_jH_k + \dots \quad (1)$$

i, j, k indices stand for x, y, z , axes.

The structure, at room temperature of all the orthoferrites, with the exception of $SmFeO_3$, is represented by the magnetic point group¹⁴:

$$E, RC_{2x}, RC_{2y}, C_{2z}, R\sigma_x, R\sigma_y, \sigma_z, I,$$

where R is the time-reversal element.

Because the energy is invariant under operation with the elements of the magnetic point group, the number of the coefficients is reduced to the following:

$$\sigma_z(0), \chi_{xx}, \chi_{yy}, \chi_{zz}, C_{xxz}, C_{yyz}, C_{zzz}.$$

For $SmFeO_3$ the point group and coefficients are the same with the indices x and z interchanged.

The components of the total magnetization $\boldsymbol{\sigma}(\mathbf{H})$ are given by¹⁷

$$\sigma_i(H) = \partial E / \partial H_i. \quad (2)$$

Thus the coefficients χ_{ii} can be interpreted as the susceptibility components along the principal axis $-\chi_x, \chi_y, \chi_z$. C_{ijk} as the terms of second-order susceptibility tensor, whereas $\sigma_i(0)$ is the ferromagnetic moment of the crystal. The S.I.A. mechanism is represented by the

¹⁷ L. D. Landau and E. M. Lifshitz, *Electrodynamics of Continuous Media* (Pergamon Press, Inc., New York, 1960), p. 147.

* The research reported in this document has been sponsored in part by the Aeronautical Systems Division, AFSC, through the European Office, Aerospace Research, U. S. Air Force.

¹ H. Forestier and G. Guiot, *Compt. Rend.* **230**, 1844 (1950).

² R. Pauthenet and P. Blum, *Compt. Rend.* **239**, 33 (1954).

³ M. A. Gilleo, *J. Chem. Phys.* **24**, 1239 (1956).

⁴ G. H. Jonker, *Physica* **22**, 707 (1956).

⁵ R. M. Bozorth, V. Kramer, and J. P. Remeika, *Phys. Rev. Letters* **1**, 3 (1958).

⁶ R. C. Sherwood, J. P. Remeika, and H. J. Williams, *J. Appl. Phys.* **30**, 217 (1959).

⁷ H. Watanabe, *J. Phys. Soc. Japan* **14**, 511 (1959).

⁸ C. Kuroda, T. Miyadai, A. Naemura, N. Niizeki, and H. Takata, *Phys. Rev.* **122**, 446 (1961).

⁹ S. Geller and E. A. Wood, *Acta Cryst.* **9**, 536 (1956).

¹⁰ S. Geller, *J. Chem. Phys.* **24**, 1236 (1956).

¹¹ W. C. Koehler and E. O. Wollan, *Phys. Chem. Solids* **2**, 100 (1957).

¹² W. C. Koehler, E. O. Wollan, and N. K. Wilkinson, *Phys. Rev.* **118**, 58 (1960).

¹³ R. M. Bozorth, *Phys. Rev. Letters* **1**, 362 (1958).

¹⁴ D. Treves, *Phys. Rev.* **125**, 1843 (1962).

¹⁵ I. E. Dzyaloshinsky, *Phys. Chem. Solids* **4**, 241 (1958).

¹⁶ T. Moriya, *Phys. Rev.* **120**, 91 (1960).

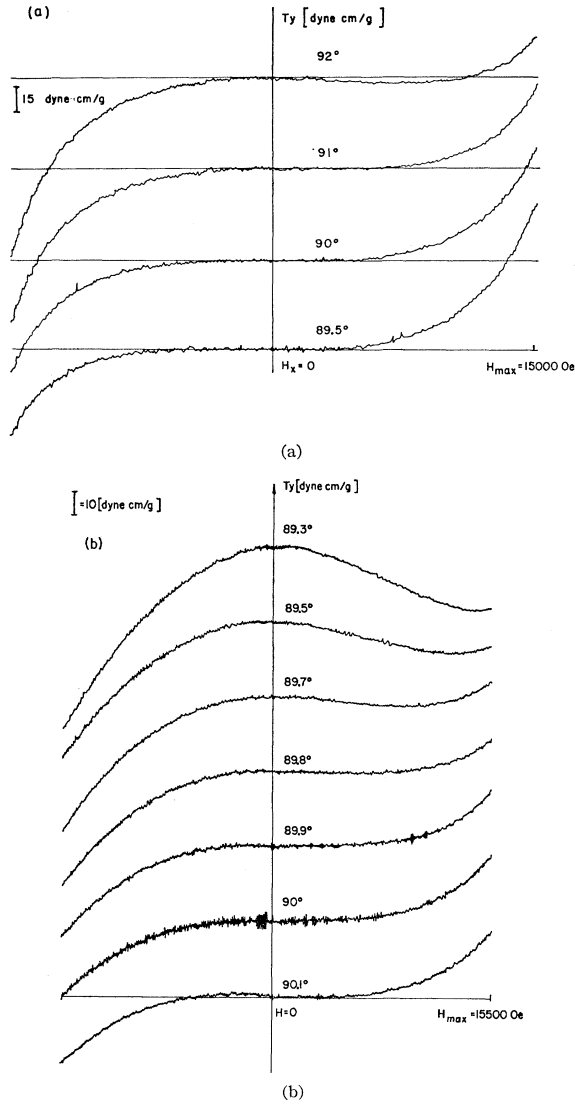


FIG. 1. The torque curves T_y , given as a function of H_x . (a) Measurements on a YbFeO_3 single crystal (18.3 mg) (b) on a HoFeO_3 single crystal (13.5 mg). As the susceptibility difference $\chi_z - \chi_x$ for HoFeO_3 is greater than that for YbFeO_3 , a small deflection in aligning the crystal distorts the antisymmetric curve much more than in the case of YbFeO_3 . The angles shown are measured from the x axis. The relative accuracy is $\pm 0.1^\circ$.

Hamiltonian

$$E_s = \lambda \boldsymbol{\sigma}_1 \cdot \boldsymbol{\sigma}_2 - \mathbf{H} \cdot (\boldsymbol{\sigma}_1 + \boldsymbol{\sigma}_2) - K(\cos^2 \delta_1 + \cos^2 \delta_2). \quad (3)$$

The first term is the isotropic superexchange interaction, the second is the energy of the interaction with the applied field and the third is the magnetocrystalline anisotropy energy. K is the anisotropy constant and $\delta_{1,2}$ are the angles between the magnetizations and the preferred crystallographic directions of the two sublattices, respectively. The symmetry of the crystal requires the value of the constant K , to be equal for the two sublattices.¹⁴ The Hamiltonian for the A.S.E.

TABLE I. The calculated values of the coefficients of the energy series expansion according to the two mechanisms studied. The expressions are correct within the approximation $\gamma_0 \ll 1$. See text for notations.

	Single-ion anisotropy model	Antisymmetric exchange model
$\sigma_z(0)$	$K \sin 2\alpha / H_e$	$D\sigma_0^2 / H_e$
χ_x	$K \sin^2 2\alpha / 4H_e^2 \cos 2(\alpha - \gamma_0)$	$\sigma_0^4 D^2 / 4K_b H_e^2$
χ_y, χ_z	σ_0 / H_e	σ_0 / H_e
C_{zzz}	$\sigma_0 \sin 2\alpha [\cos(2\alpha - \gamma_0) - K \sin^2 2\alpha / 8H_e \sigma_0]$	$\sigma_0^3 D(1 - \sigma_0^2 D^2 / 8K_b H_e)$
C_{yyy}, C_{zzz}	$4H_e^2 \cos^2 2(\alpha - \gamma_0)$	$4K_b H_e^2$
C_{yyz}, C_{zzz}	$-K \sin 2\alpha / 8H_e^3$	$-D\sigma_0^2 / 8H_e^3$

mechanism is taken as:

$$E_a = \lambda \boldsymbol{\sigma}_1 \cdot \boldsymbol{\sigma}_2 - \mathbf{H} \cdot (\boldsymbol{\sigma}_1 + \boldsymbol{\sigma}_2) - \mathbf{D} \cdot (\boldsymbol{\sigma}_1 \times \boldsymbol{\sigma}_2) - (K_b / \sigma_0^2)(\sigma_{1x}^2 + \sigma_{2x}^2). \quad (4)$$

Here $\sigma_0 = |\boldsymbol{\sigma}_1| = |\boldsymbol{\sigma}_2|$. The fourth term is the magneto-crystalline anisotropy energy with easy direction of magnetization equal for both sublattices and parallel to the x axis. This term is required to describe the anisotropy in the plane $y=0$. The values C_{ijk} , χ_i , and $\sigma_i(0)$ are obtained theoretically from the derivatives of the Hamiltonian E at the equilibrium position.

$$\sigma_i(0) = \left. \frac{\partial E}{\partial H_i} \right|_{H=0}, \quad \chi_i = \left. \frac{\partial^2 E}{\partial H_i^2} \right|_{H=0}, \quad (5)$$

$$C_{ijk} = \left. \frac{\partial^3 E}{\partial H_i \partial H_j \partial H_k} \right|_{H=0}.$$

The calculated coefficients of the energy series expansion according to the two models are summarized in Table I. In this table, $H_e = \lambda \sigma_0$. γ_0 , is the canting angle at $H=0$ and α is the angle between the preferred crystallographic directions of magnetization and the x axis (for SmFeO_3 , the z axis). Experimentally these constants are obtained from torque measurements by the following equations:

$$T_i = (\boldsymbol{\sigma}(\mathbf{H}) \times \mathbf{H})_i = \frac{\partial E}{\partial H_j} \cdot H_k - \frac{\partial E}{\partial H_k} \cdot H_j, \quad (6)$$

T_i —being the i th torque component. The explicit form of these equations is:

$$T_x = H_y(\sigma_z(0) + \chi_z H_z + 3C_{zzz} H_z^2 + C_{xxz} H_x^2 + C_{yyz} H_y^2) - H_z(\chi_y H_y + 2C_{yyz} H_y H_z), \quad (7a)$$

$$T_y = -H_x(\sigma_z(0) + \chi_z H_z + 3C_{zzz} H_z^2 + C_{xxz} H_x^2 + C_{yyz} H_y^2) + H_z(\chi_x H_x + 2C_{xxz} H_x H_z), \quad (7b)$$

$$T_z = H_x(\chi_y H_y + 2C_{yyz} H_y H_z) - H_y(\chi_x H_x + 2C_{xxz} H_x H_z). \quad (7c)$$

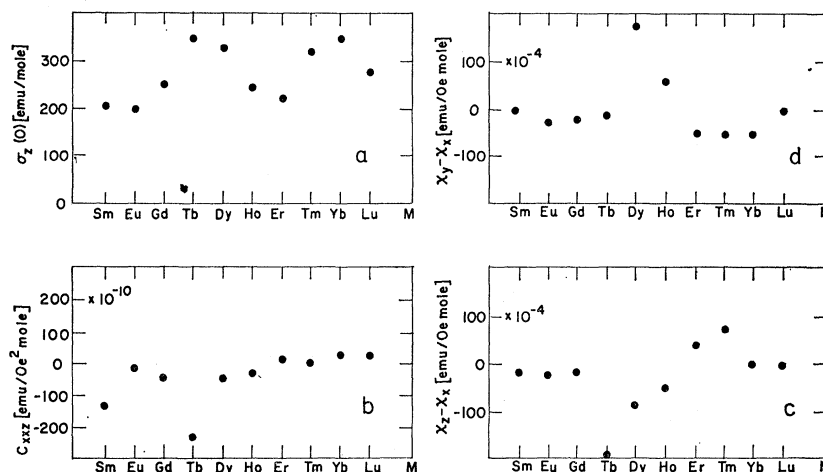
By comparing the theoretical and experimental values, it was found¹⁴ that in the three orthoferrites with nonmagnetic rare-earth ions YFeO_3 , LaFeO_3 , and

TABLE II. Values of the various coefficients as obtained from torque measurements.*

	$\sigma_z(0)$ (emu/mole)	$C_{xxx} \times 10^{10}$ (emu/Oe ² mole)	$C_{yyz} \times 10^{10}$ (emu/Oe ² mole)	$C_{zzz} \times 10^{10}$ (emu/Oe ² mole)	$(\chi_z - \chi_x) \times 10^4$ (emu/Oe mole)	$(\chi_z - \chi_y) \times 10^4$ (emu/Oe mole)	$(\chi_y - \chi_x) \times 10^4$ (emu/Oe mole)
YFeO ₃ ^b	232	-32.6 ÷ -47.2	<2.0	<2.0	-13.5 ÷ -15.4	<0.1	-13.5 ÷ -19.9
LaFeO ₃ ^b	243	31.9	-2.9 ÷ -4.1	-18.2	3.2	<0.2	4.3
LuFeO ₃ ^b	279	25.0	<0.5	<5.0	3.6	<0.3	2.2 ÷ 5.3
YbFeO ₃	340 ÷ 358	29.6 ÷ 32.4	4		5.5 ÷ 6.6	29 ÷ 39.3	-38.5 ÷ -53.2
TmFeO ₃	320 ÷ 324	5.7 ÷ 7.3	1 ÷ 3.9		74 ÷ 81.5	125 ÷ 134	-54.2
ErFeO ₃	228 ÷ 233	15.3 ÷ 20.1	2.0 ÷ 5.5		39.6 ÷ 41.8	81.0 ÷ 89.3	-48.8
HeFeO ₃	236 ÷ 250	-23.0 ÷ -28.7	-1 ÷ -2		-45.7 ÷ -53.2	-102 ÷ -115	61.0
DyFeO ₃	330	-47.4	-5.3		-84.3 ÷ -89.2	-274 ÷ -279	176
TbFeO ₃	340 ÷ 356	-222 ÷ -239	-3.5 ÷ -8		-192 ÷ -205	-178 ÷ -184	-12.5
GdFeO ₃	257	-47.0	<1		-13.7 ÷ -15.5	1.0 ÷ 1.6	-19.6
EuFeO ₃	198 ÷ 204	-10.3 ÷ -15.1	<1		-17.7 ÷ -18.7	5.2 ÷ 7.9	-20.5
SmFeO ₃	$\sigma_x(0)$ 202 ÷ 210	$C_{zzz} \times 10^{10}$ -126 ÷ -149	$C_{yyz} \times 10^{10}$ <1		16.2 ÷ -28.0	-19.3	0.2 ÷ 1.2

* The numbers given are the extreme values observed in various crystals.
^b Published results see Ref. 14.

FIG. 2. Coefficients of the energy series expansion evaluated from torque measurements (a) the values of $\sigma_z(0)$; (b) the values for C_{xxx} ; (c) the values for $\chi_z - \chi_x$; (d) the values for $\chi_y - \chi_x$.



LuFeO₃ the dominating interaction is the A.S.E. one.¹⁸

The purpose of this work is to study the other orthoferrites of this family with magnetic rare-earth ions and to see if here also one obtains the same results.

EXPERIMENTS AND RESULTS

An automatic recording torque magnetometer with a sensitivity of 10^{-2} dyn·cm was used for these measurements. The magnetic field was continuously measured with a Hall probe (HR-31 Halltron O.S, Inc.) and curves of torque versus field plotted on an x - y recorder. The systematic error, which arises from the nonlinearity of the Hall probe in the wide range (0–15 000 Oe) of the applied magnetic field, was measured with a rotating-coil Rawson gaussmeter. The calculations were corrected according to it.

In order to minimize the influence of imperfections in

¹⁸ The expression for C_{zzz} in Ref. 5 was incorrect. The authors wish to thank Dr. G. F. Herrman for pointing out this mistake. It should be mentioned that this mistake does not affect any of the conclusions drawn in that work.

the crystals the measurements were carried out on small, optically selected crystals (4–20 mg). Only those with a relatively high coercive force and with square hysteresis curves were actually measured. The crystals were kindly supplied by J. P. Remeika from Bell Telephone Laboratories, Inc.

$\sigma_z(0)$ is calculated from the slope of the curves:

$$T_i = \sigma_z(H)H_j \quad (i, j \neq z)$$

at the point $H=0$.

The susceptibility differences, $\chi_i - \chi_j$ are obtained from torque measurements with the magnetic field applied in directions not parallel to the crystallographic axes.

The constant C_{xxx} is determined from the torque T_y as a function of the field H_x (Eq. 7b). In the range of the measuring fields $|\chi_z - \chi_x| \gg HC_{xxx}$, thus small deviations of the magnetic field from the x axis will add to the antisymmetric curve $T_y = C_{xxx}H_x^3$ a symmetric torque due to the susceptibility terms [Eq. (7b)]. This can be clearly seen in Fig. 1. The alignment of the

TABLE III. Calculated values of C_{yyz} , the superexchange, antisymmetric exchange, and anisotropy fields, $2K_b/\sigma_0$ and $2K/\sigma_0$ for the two models.

	$H_e \times 10^{-6}$ (Oe)	$D\sigma_0 \times 10^{-5}$ (Oe)	$2K_b/\sigma_0$ (Oe)	$C_{yyz} \times 10^{12}$ (emu/Oe ² mole)	$(2K/\sigma_0) \times 10^{-5}$ (Oe)	α (deg)	$C_{yyz} \times 10^{12}$ (emu/Oe ² mole)
YFeO ₃	6	1	370	-0.8	-0.8
LaFeO ₃	6	1	470 ^a	-0.8	0.8	$\approx 45^\circ$	-0.8
YbFeO ₃	4.2	1.1	770 ^a	-2.2	1.4	$\approx 45^\circ$	-1.4
TmFeO ₃	4.2	1.1	830 ^a	-2.2	1.4	$\approx 45^\circ$	-1.6
ErFeO ₃	4.3	0.7	390 ^a	-2.2	1.4	$\approx 45^\circ$	-2.2
HoFeO ₃	4.3	0.7	500	-1.6	-1.6
DyFeO ₃	4.4	1.1	630	-2.2	-1.6
TbFeO ₃	4.4	1.1	540	-2.2	-1.4
GdFeO ₃	4.4	0.8	360	-1.6	-1.4
EuFeO ₃	4.5	0.6	410	-1.2	-1.4
SmFeO ₃	4.6	0.6	170	$C_{yyz} \times 10^{12}$ -1.2	$C_{yyz} \times 10^{12}$ -1.4

^a As $\sigma_0^3 D^2 / 8K_b H_e < 1$ two values for $2K_b/\sigma_0$ are obtained. In the table only the lower one is given.

magnetic field is carried out by minimizing the symmetric contribution to the torque curve.

C_{yyz} is determined from the measurement of T_x in an applied field H_y [Eq. (7a)].

It seems from Eq. (7a) that C_{zzz} can be determined from the torque T_x as a function of an applied field in the plane $x=0$ (not along one of the principle axes). Actually the contribution of the susceptibility to the torque in this plane is so large in comparison to $C_{zzz}H^2$, that the value for C_{zzz} can not be derived.

The contribution of $\sigma_z(0)$ to the torque in the planes $x=0$, $y=0$ is several orders of magnitude larger than that of the nonlinear terms; thus in order to measure these, $\sigma_z(0)$ is canceled by a steady current flowing in a bucking coil rigidly attached to the crystal holder. The same coil was used to calibrate the torquemeter. The constant of the coil was calculated from its geometrical dimensions and calibrated against nickel in a vibrating sample magnetometer.

The measurements described are valid for SmFeO₃ after interchanging the x and z axes.

The nonlinear terms in the torque are taken as positive if they have the same sign as the linear one.

The measurements have been done on 3-4 single crystals of each of the rare-earth orthoferrites with the exception of GdFeO₃ and DyFeO₃ of which only one good single crystal was available.

The experimental results for nine orthoferrites, are summarized in Table II and described in Fig. 2. The values given are the extreme ones observed in the measurements. The small variation of the results indicated that the phenomenon arises from an intrinsic property of the crystalline structure.

DISCUSSION

Contrary to La³⁺, Y³⁺, and Lu³⁺ the rare-earth ions studied here are paramagnetic. Thus in order to analyze the results given in Table II with respect to the mechanism responsible for the canted structure, it is necessary to examine the extent of the influence of M³⁺ ions on

the coefficients C_{xxx} , which are the main criterion for deciding which of the models is the dominating one.

The experimental data (Table II) show that the spontaneous magnetization at room temperature for the nine orthoferrites studied are approximately equal to those for LaFeO₃, YFeO₃, and LuFeO₃, indicating that the contribution to the ferromagnetic moment by the paramagnetic rare-earth ions in the internal field of the iron sublattice is small.

It thus follows that the coupling at room temperature between the sublattices of Fe³⁺ and M³⁺ ions is negligible leaving the rare-earth ions in an unperturbed paramagnetic state. Within this approximation the rare-earth ions assembly is invariant under time reversal and therefore does not contribute to the C_{ijk} terms. Indeed all the values for C_{xxx} and C_{yyz} are similar, with the exception of SmFeO₃ and TbFeO₃, in spite of large changes in magnetic moments of the various rare-earth ions.

All the following discussion is carried out following this assumption, that the C_{ijk} terms depend only on the Fe³⁺-ion sublattices.

The anisotropy fields and the coefficient C_{yyz} for each of the models, the antisymmetric exchange field, $D\sigma_0$ in the A.S.E. model and the angle α between the easy direction of magnetization and the x axis, which appears in the S.I.A. model, are calculated from the equations given in Table I by introducing the measured values for $\sigma_z(0)$ and C_{xxx} . The results are summarized in Table III.

The exchange field H_e was calculated from the Curie temperature¹⁹ T_c

$$H_e = 3KT_c / (S+1)g\mu_B. \quad (10)$$

An important point in examining the models, is the sign of¹⁴ C_{xxx} (for SmFeO₃, C_{zzz}). In the A.S.E. model C_{xxx} gets negative values when $\sigma_0^3 D^2 / 8K_b H_e > 1$. In the

¹⁹ Differential thermal analysis and Mössbauer studies in rare-earth orthoferrites. M. Eibshutz, G. Gorodetsky, S. Shtrikman, and D. Treves, J. Appl. Phys. Suppl. 35, 1071 (1964).

S.I.A. model the C_{xxz} is always positive. Table II shows that C_{xxz} for HoFeO_3 , DyFeO_3 , TbFeO_3 , GdFeO_3 , EuFeO_3 and C_{zzz} for SmFeO_3 is indeed negative, indicating that the dominant mechanism in the orthoferrites is the A.S.E. one. An additional point that rules out the S.I.A. mechanism even in YbFeO_3 , TmFeO_3 and ErFeO_3 in which C_{xxz} is positive, is the high value of the anisotropy constant ($K \approx 15 \times 10^8$ erg/mole), which is larger than that expected for Fe^{+3} ion in a similar configuration.¹⁴

The calculated coefficients C_{yyz} for both mechanisms are practically equal and lower than the sensitivity threshold of the torquemeter. Although C_{yyz} in some of the materials appears to be higher than the predicted ones, because of the low measured values and their large spread, no significant conclusions can be drawn.

The ions of Gd^{3+} have a basic level 8S_7 , lie on an approximately cubic lattice and are therefore isotropic.³ It can be assumed that in GdFeO_3 the anisotropy in the

susceptibility is due mostly to the iron ions. Evidence to this assumption is the isotropy of the susceptibility in the plane perpendicular to the antiferromagnetic axis, in contrast to the other orthoferrites with paramagnetic rare earth. One can then use the measured anisotropy of the susceptibility in GdFeO_3 as an additional check for the dominant mechanism. Experimentally (see Table II) $\chi_x > \chi_z$. This is inconsistent with the S.I.A. model as shown from Table I.

According to the A.S.E. model this relation between the susceptibilities occurs for $\sigma_0^3 D^2 / 4K_b H_e > 1$ which is actually the case in GdFeO_3 , as can be seen from Table III. This is an additional evidence that the dominating mechanism is the A.S.E. one.

ACKNOWLEDGMENT

We would like to thank Dr. S. Shtrikman for helpful discussions.

F Band in Isotopically Enriched LiF^\dagger

HERBERT RABIN AND MICHAEL REICH*

U. S. Naval Research Laboratory, Washington, D. C.

(Received 4 February 1964)

The effect of isotopic composition on the optical absorption spectrum of the F center in LiF has been investigated. The results of measurements on single crystals of x-ray irradiated Li^6F (almost 96% lithium-6) and Li^7F (almost 100% lithium-7) indicate that the average F -band width at half-maximum in the former is larger by about 3% at liquid-helium temperature, and by about 1% at room temperature. Theory shows that the half-widths in the two isotopic forms vary inversely as the fourth root of the mass of the alkali ions at low temperature, and as the temperature is increased the predicted half-width difference monotonically decreases to zero. The predicted half-width difference at low temperatures is about 4%, and at room temperature about 1%, both in reasonable agreement with experiment. At both room and liquid-helium temperatures the position of the F -band maximum in Li^7F is slightly displaced to higher energy than in Li^6F . The peak-position shift is in approximate agreement with the contributions arising from the difference in alkali mass and lattice constant of the two crystals as estimated at low temperature.

I. INTRODUCTION

THE F center, an electron bound to an anion vacancy, has been the subject of numerous experimental and theoretical studies in alkali-halide crystals.¹⁻⁷ The principal transition of the F center from its

[†] A preliminary account of this work was presented at the New York American Physical Society Meeting, January 1964, Bull. Am. Phys. Soc. **9**, 89 (1964).

* Present address: Swarthmore College, Swarthmore, Pennsylvania.

¹ R. W. Pohl, Proc. Phys. Soc. (London) **49**, 3 (1937), extra part.

² F. Seitz, Rev. Mod. Phys. **18**, 384 (1946).

³ F. Seitz, Rev. Mod. Phys. **26**, 7 (1954).

⁴ D. L. Dexter, in *Solid State Physics*, edited by F. Seitz and D. Turnbull (Academic Press Inc., New York, 1958), Vol. 6.

⁵ J. J. Markham, Rev. Mod. Phys. **31**, 956 (1959).

⁶ B. S. Gourary and F. J. Adrian, in *Solid State Physics*, edited by F. Seitz and D. Turnbull (Academic Press Inc., New York, 1960), Vol. 10.

⁷ J. H. Schulman and W. D. Compton, *Color Centers in Solids* (Pergamon Press, Inc., New York, 1962).

ground state gives rise to the well-known F -band absorption. This band is approximately Gaussian in shape, and its spectral location is characterized by the particular crystal, typically occurring in the visible or ultraviolet ranges. Normally, half-widths of the F band are found in the range 0.4–0.7 eV in the vicinity of room temperature. Upon lowering the temperature there is appreciable narrowing of the bandwidth and shifting of the spectral position of the band maximum to higher energies. The breadth of the F band is attributed to interaction with vibrational modes of the lattice, and even at low temperature the F band retains appreciable half-widths, normally over 50% of the room-temperature value, owing to zero-point vibration of the lattice.

The interaction of the F center with vibrational phonons has been treated theoretically in the limit of